Experimental Study of Design Parameters in Silicon Micropillar Array Solar Cells Produced by Soft Lithography and Metal-Assisted Chemical Etching

Jae Cheol Shin, Debashis Chanda, Winston Chern, Ki Jun Yu, John A. Rogers, *Fellow, IEEE*, and Xiuling Li, *Senior Member, IEEE*

***Abstract*—Solar cells, consisting of core-shell p-n junction silicon micropillars on a thin membrane fabricated using soft lithography and metal-assisted chemical etching, are studied as a function of geometrical designs. Significant enhancement in absorption rate is found without much dependence on the pillar diameters in the range of 0.5–2 μm. However, the short-circuit current increases continuously with diameter, which is inversely proportional to the total surface area for a fixed diameter/pitch pillar array. This study provides unambiguous evidence that surface recombination is the dominant loss mechanism in nanowire- or micropillar-based solar cells.**

***Index Terms*—Etching, nanopatterning, photovoltaic cells, semiconductor nanostructures.**

I. Introduction

HIGH aspect ratio semiconductor micro- or nanoscale structures have allowed new design concepts and demonstrated performance enhancement for various types of devices including solar cells, batteries, detectors, and thermoelectric systems [1]–[3]. Micropillar or nanowire arrays have been of interest for photovoltaic applications because of the enhanced light trapping inherent to pillar or wire geometry and high carrier collection efficiency by separating the path for light absorption and carrier collection using core-shell p-n junction [4], [5] and increasing the junction area. These advantages can significantly reduce the cost of high-efficiency solar cells by using less or inexpensive silicon (Si) substrates which have short optical path and minority carrier diffusion length [5]–[7]. High aspect ratio micropillar array can experimentally be produced by either metal-catalyzed vapor–liquid–solid (VLS) growth [8] or top-down dry etching [5]. In-depth studies have been carried out on VLS-grown Si nanowire solar cells and efficiencies as high as $\sim$4% have been reported [1], [9], [10]. However, carrier recombination within the depletion region or at the surface of VLS nanowires due to metal catalyst contamination related deep levels could limit the overall efficiency. Dry etch, on the other hand, is susceptible to ion-induced surface damage. Recently, metal-assisted chemical etching (MacEtch) [11]–[13], a wet but directional etching method, has been used to produce Si nanowires with aspect ratio that is primarily limited by etching time. MacEtch is free of surface damage compared with dry etching processes because there is no high-energy ions involved. MacEtch does not cause metal contamination compared with the VLS method because it takes place at room temperature and the metal catalyst cannot be incorporated in Si. In addition, MacEtch is scalable to whole wafer scale with lateral resolutions as high as 10 nm through various metal-patterning techniques such as superionic solid state stamping [14], colloidal lithography [15]–[17], electron beam lithography [18], or soft lithography [19]. Wang *et al*. have recently demonstrated Si nanowire array solar cells using MacEtch with nanosphere lithography; however, the efficiency measured was only 1.47%, possibly due to the porous top surface of the nanowires produced [20].

The geometry of silicon nanowire or micropillar structures has been theoretically studied to optimize absorption and collection efficiency, thus the performance of solar cells. For example, using a full-wave finite-element method [4], [6], [21], the authors found that although there is a wide window in terms of the Si nanowire diameter and array pitch for improving solar energy harvesting, increasing pillar diameter or period first led to an increase and then a decrease in absorption efficiency for a fixed diameter to period ratio (D/P). The authors attributed the trend to the tradeoff between the light transmission suppression and the light reflection enhancement. However, few systematic experimental studies on the effect of micropillar diameter, pitch, and height have been reported [5], probably due to processing challenges.

In this paper, combining soft lithography patterning of Au with MacEtch, we systematically study the photovoltaic responses of the solar cells consisting of extremely uniform, ordered, and solid Si micropillar arrays with respect to pillar geometry. We report the open-circuit voltage $V_{\rm oc}$, short-circuit current density $J_{\rm sc}$, fill factor (FF), and efficiency η of the micropillar solar cells, as well as absorption rate, as a function of pillar

Manuscript received November 5, 2001; revised December 3, 2011; accepted December 13, 2011. Date of publication January 27, 2012; date of current version March 16, 2012. This work was supported in part by the Department of Energy Division of Materials Science under Award DEFG02-07ER46471, by the Frederick Seitz Materials Research Laboratory at the University of Illinois at Urbana-Champaign, and by the National Science Foundation under Award 0749028 (CMMI).

J. C. Shin, W. Chern, K. J. Yu, and X. Li are with the Department of Electrical and Computer Science Engineering, University of Illinois, Urbana-Champaign, IL 61801 USA (e-mail: xiuling@illinois.edu).

D. Chanda and J. A. Rogers are with the Department of Materials Science and Engineering, University of Illinois, Urbana-Champaign, IL 61801 USA (e-mail: jrogers@uiuc.edu).

Color versions of one or more of the figures in this paper are available online at http://ieeexplore.ieee.org.

Digital Object Identifier 10.1109/JPHOTOV.2011.2180894

2156-3381/$31.00 © 2012 IEEE

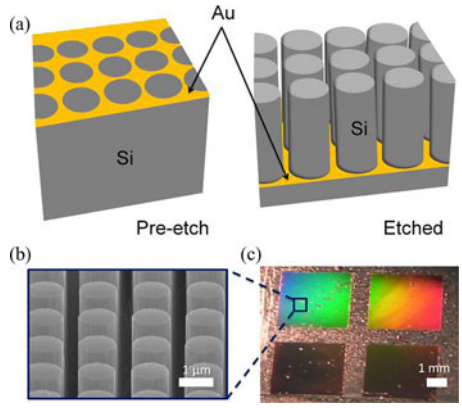

Fig. 1. (a) Schematic illustration of the MacEtch mechanism, where the metal pattern (Au mesh in yellow color) descends by etching Si directly underneath resulting in a 3-D Si structure (Si pillars are in gray color). (b) 45° tilted SEM image of Si micropillar array produced by Au-MacEtch. (c) Optical image of MacEtched micropillar arrays. Each square consists of pillars of different diameters.

diameter and spacing, measured under air mass 1.5 (AM 1.5, 100 mW/cm^2) illumination.

II. Experimental Procedure

p-type Si (1 0 0) (ρ = 1–10 Ω·cm) substrate was used to generate micropillar array using MacEtch. Au was used as the MacEtch catalyst because it has been known to produce solid and smooth surface compared with other catalysts [14], [18]. Au mesh patterns of a variety of dimensions were generated by soft lithography with a liftoff process [19]. The MacEtch solution to produce solid micropillar was a mixture of concentrated HF, H_2O_2, and ethanol (EtOH). In MacEtch, the oxidizing agent (i.e., H_2O_2) generates free holes (h^+) when catalyzed by the metal. The holes oxidize Si at the metal–Si interface and HF dissolves oxidized Si [12]. As a result, the material directly underneath the metal is preferentially removed and the metal descends into the semiconductor, as illustrated in Fig. 1(a). The etch rate for Si can be as fast as >3 μm/min and the etching direction and surface roughness can be controlled by etchant concentration [14]. Fig. 1(b) shows a scanning electron microscope (SEM) image of Si micropillars generated by Au-MacEtch with 1-μm diameter and 1.66 μm in pitch. The volume ratio of the etching solution was 5, 1, and 1 for concentrated HF, H_2O_2, and EtOH, respectively. After MacEtch, the Au catalyst was removed in wet etching solution (e.g., gold etchant TFA, Transene Inc.) and the sample was further cleaned with RCA (Radio Corporation of America) and HF solutions. Shown in Fig. 1(c) is an optical image of micropillar arrays with each square (4 mm × 4 mm) having a different diameter showing different reflectivity.

Fig. 2 illustrates the micropillar array solar cell p-n junction and metal contact schemes (left: cross section; right: top view). The n^+ Si shell on the surface of p-Si micropillar was formed by thermal diffusion of solid phosphorus doping source (P_2O_5) in a furnace at 1000 °C for 7 min. The thickness of n^+ shell was estimated to be ~200 nm using the Deal and Grove model. The backside of the sample was protected by 1-μm-thick SiO_2 during thermal treatment and cleaned with HF afterward. Similarly,

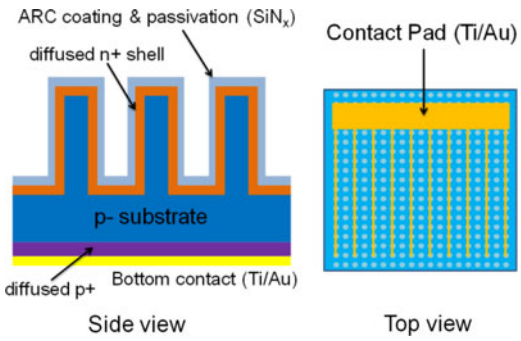

Fig. 2. Schematic illustrations of the solar cell structure, (left) cross section and (right) top view, with the core-shell junction and metal contact scheme indicated. The pillar height and tray thickness are not to scale.

the p^+ contact layer on the backside of sample was thermally diffused using solid boron doping sources (B_2O_3) for 20 min at 1000 °C while the top side of sample was protected by SiO_2. The sample was cleaned again with HF and RCA after thermal diffusion. 80 nm of SiN_x was deposited on the micropillar surface for antireflective (AR) coating as well as surface passivation. Note that the SiN_x layer was not optimized for passivation in our case and surface recombination should be further reduced by optimizing the film composition and morphology [9], [22].

Finger-shaped top metal contact area was lithographically defined by opening the SiN_x coating and Ti/Au (15 nm/300 nm) metal contact was sputtered onto the opened area and followed by a liftoff process [see Fig. 2(b)]. Finally, Ti/Au (15 nm/300 nm) metal contact was deposited on the backside of solar cells.

Absorption spectrum of the micropillar array was measured in the range of 0.45–1.0 μm. Normal incidence light was shined onto the samples, reflected by the Au on the backside of the sample (i.e., transmission is zero), and then collected by a detector positioned at ~0.5 cm. This small gap between the sample and the detector probably results in an underestimate of the absorption rate, because a small portion of reflected light may not be collected into the detector due to scattering. Short-circuit current I_{sc} and open-circuit voltage V_{oc} were measured using a solar simulator which illuminates light equivalent to air mass 1.5 (AM 1.5, 100 mW/cm^2). Short-circuit current density J_{sc} and conversion efficiency η were calculated using top planar area of the solar cell excluding finger-patterned metal area.

III. Results and Discussion

Fig. 3 shows SEM images of micropillar array generated from single crystalline p-type Si (1 0 0) substrate (ρ = 1–10 Ω·cm). The diameters of the micropillar arrays are 0.54 [Fig. 3(a)], 0.74 (not shown), 0.94 (not shown), and 2 μm [Fig. 3(b)]. The diameter/pitch (D/P) ratio of all micropillar arrays is 0.51 ± 0.02 and height is 10 ± 2 μm [see Fig. 3(c)], respectively. The fixed D/P ratio and height provide a platform for systematic evaluation of diameter dependence of solar cell performance with the same total absorbing volume. To confirm the core-shell radial junction structure, the tips of the 0.54-μm-diameter micropillars were cut using focused ion beam and wet-etched in heated (60 °C) potassium hydroxide (KOH) solution for 2 s.

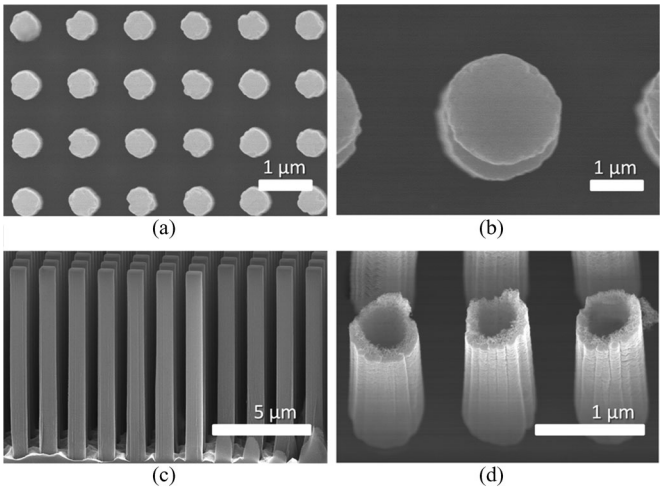

Fig. 3. Top SEM views of the (a) smallest (0.54 μm) and (b) largest (2 μm) diameter pillars used in this study under the same magnification. (c) 85° tilted SEM view of a micropillar array with highly vertical, nontapered sidewalls. (d) 5° tiled SEM view of hollow pillars after selectively removing the p-type cores leaving behind the n^+ cylindrical shells by dipping in KOH solution for 2 s.

Because the etch rate of p-type Si is much faster than that of the n-type Si in this solution [23], the core-shell micropillars are reduced to a hollow structure after selectively removing the p-Si core, as shown in Fig. 3(d).

Fig. 4(a) and (b) shows the absorption spectra and total absorption rate for Si cells with various geometrical designs as indicated. The pillar based cells consist of a 10-μm-tall micropillar array sitting on a 40-μm-thick Si membrane substrate. The reference planar Si cell thickness is 50 μm. In the wavelength range measured from 0.45 to 1.0 μm, the total absorption rate of planar Si increases from 72% to 88% as a result of SiN_x AR coating. Converting the top 10 μm from planar sheet to periodic pillar arrays increases the absorption rate to more than 94%. Note that the absorption rate shows slight increase as the pillar diameter becomes smaller [see Fig. 4(b)], but the difference is insignificant (<2%).

Fig. 5(a) and (b) show the photovoltaic responses of the processed solar cells as a function of Si membrane substrate thickness, where a micropillar array with the pillar diameter at 2-μm and height at 10 μm sits on top of the Si membrane substrate. The junction geometry, as illustrated in Fig. 2, consists of a core-shell p-n junction in the pillars. It can be seen that V_{oc}, J_{sc}, and η of the micropillar array solar cells increase as the substrate thickness decreases from 325 to 40 μm. This indicates that although increasing thickness naturally enhances light absorption, light-generated carriers may not contribute to the overall efficiency probably due to limited minority carrier diffusion length and bulk recombination (e.g. Auger) as previously reported [6], [24]. For planar Si cell, the optimum solar cells thickness is around 90 μm for $\rho = 1\ \Omega$·cm and this thickness decreases for Si with lower resistivity [25]. In contrast, for the micropillar cell geometry studied here, the optimum total thickness is less than 40 μm, thanks to the light-trapping effect of the micropillar array. Further reducing the thickness beyond

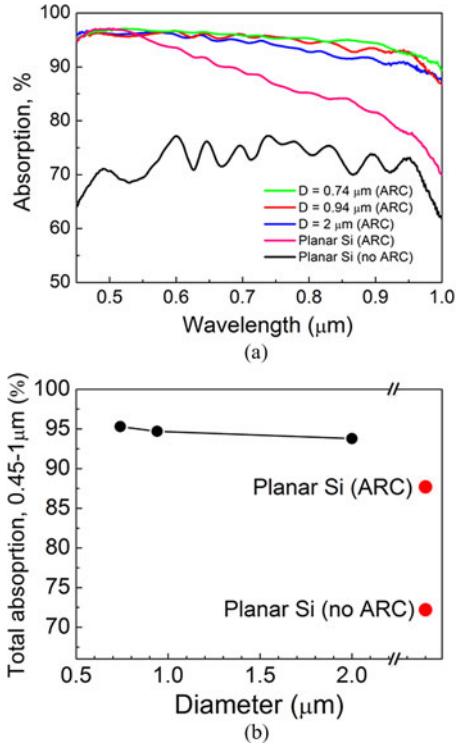

Fig. 4. Absorption spectra (a) and total absorption rate of (b) Si micropillar array based structures of various diameters, as well as the reference planar structures, in the wavelength range from 0.45 to 1 μm.

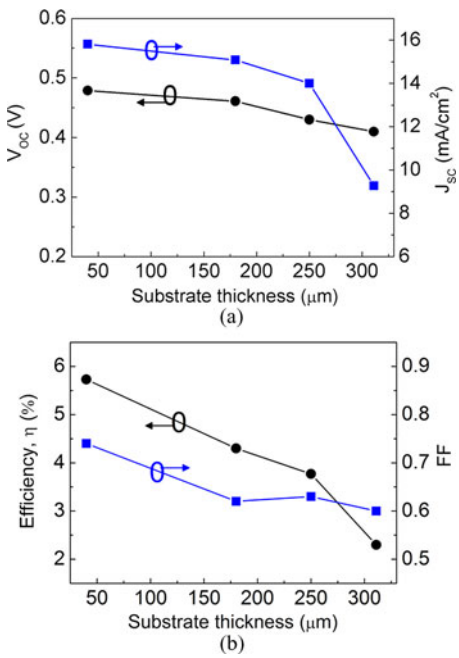

Fig. 5. (a) V_{oc} and J_{sc}, and (b) η and FF, of a 2-mm-diameter micropillar array solar cells as a function of Si membrane substrate thickness.

40 μm could not be performed due to handling difficulties in processing. The small variation of FF with thickness shown in Fig. 5(b) is probably a result of slight variation of processing condition.

Fig. 6(a) and (b) show the photovoltaic responses as a function of micropillar diameter, for the same cell geometry as in

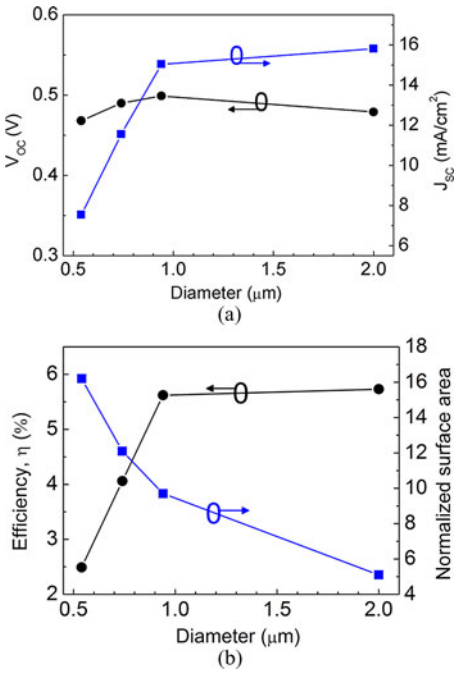

Fig. 6. (a) $V_{\rm oc}$ and $J_{\rm sc}$, and (b) η and top surface area of the micropillar-array-based solar cells as a function of pillar diameter.

Fig. 4(a) and (b) with a fixed membrane substrate thickness of 40 μm. $V_{\rm oc}$ changes from 0.47 to 0.5 V and FF (not plotted) of micropillar solar cells are between 0.69 and 0.74 for all the diameters studied. These small variations appear to be related to processing variation rather than diameter difference. However, $J_{\rm sc}$ increases almost linearly with diameter from 0.54 to 0.94 μm and then starts to level off from 0.94 to 2 μm. The total light absorption of the micropillar array is very similar (e.g., 94 $\pm$ 1%) for all diameters, as shown in Fig. 4(b). The total volume of Si after MacEtch is the same for all micropillar arrays due to the same D/P ratio and same height. Therefore, the absorption rate and total absorption volume of micropillar solar cells cannot explain the increase of $J_{\rm sc}$ with diameter. In addition, the junction depth is smaller than the minority carrier diffusion length for all structures due to the radial junction design [6], [26], even though the fractional volume of the diffused n^+ region increases with decreasing diameter.

However, surface recombination could play an important role in the $J_{\rm sc}$ of micropillar array solar cells because the highly doped Si surface area dramatically increases for high aspect ratio micropillar arrays. Fig. 6(b) shows the calculated surface area of the micropillar array in the cells studied normalized to that of the flat surface as a function of pillar diameter. Indeed, the surface area is inversely proportional to the energy conversion efficiency of the micropillar array. This indicates that surface recombination is the dominant loss mechanism limiting the efficiency of the pillar based solar cells. A 50-μm-thick planar Si membrane was fabricated under the same processing condition as a reference and the $V_{\rm oc}$, $J_{\rm sc}$, FF, and η are 0.5 V, 17.1 mA/cm^2, 0.76, and 6.8%, respectively. Although the efficiency (6.8%) of the planar solar cells at this total thickness (50 μm) still exceeds that of micropillar array (up to 5.7%), the enhanced light-trapping effect should prevail for reduced total thickness structure, as demonstrated by Garnett and Yang [5] for an 8-μm-thick structure. Moreover, by optimizing passivation schemes such as using different composition SiN_x film [22], amorphous silicon–nitrogen alloy (a-SiN_x:H) layer [9], more conforming layers to the sidewall surfaces i.e., Al_2O_3, SiC_x [22], [27], [28], or *in situ* amorphous Si coating [29], we expect the $J_{\rm sc}$ and η of micropillar solar cells exceed those of planar Si solar cells for a wide range of total thickness and different purity silicon materials.

IV. Conclusion

We have demonstrated Si solar cells consisting of MacEtch produced perfectly ordered, vertical, solid, and uniform Si micropillars of various diameters with measured energy conversion efficiency in the range of 2.5–5.7%. While approximately the same level of enhancement in absorption rate over planar structure is found for all the structures studied, $J_{\rm sc}$ continues to increase with diameters beyond theoretically predicted optimum values [21]. This is attributed to the surface area of the micropillar array which decreases with increasing diameter for the constant diameter/pitch ratio structures, confirming that surface recombination is the dominant loss mechanism in these solar cells. This observation underlines the importance of effective passivation of Si micropillar sidewalls. The implications of this study not only should help nanowire/micropillar based solar cell designs fabricated top-down using MacEch, but also shine light on bottom-up grown nanowire-based solar cells. The simplicity and controllability of MacEtch in combination with soft lithography metal patterning makes it a manufacturable technology for fabricating nanowire/micropillar-based photovoltaic cells for better light trapping or carrier collection thus overall energy conversion efficiency.

References

[1] B. Tian, X. Zheng, T. J. Kempa, Y. Fang, N. Yu, G. Yu, J. Huang, and C. M. Lieber, "Coaxial silicon nanowires as solar cells and nanoelectronic power sources," *Nature*, vol. 449, pp. 885–889, 2007.

[2] A. I. Hochbaum, R. Chen, R. D. Delgado, W. Liang, E. C. Garnett, M. Najarian, A. Majumdar, and P. Yang, "Enhanced thermoelectric performance of rough silicon nanowires," *Nature*, vol. 451, pp. 163–167, 2008.

[3] C. K. Chan, H. Peng, G. Liu, K. McIlwrath, X. F. Zhang, R. A. Huggins, and Y. Cui, "High-performance lithium battery anodes using silicon nanowires," *Nature Nano.*, vol. 3, pp. 31–35, 2008.

[4] M. D. Kelzenberg, S. W. Boettcher, J. A. Petykiewicz, D. B. Turner-Evans, M. C. Putnam, E. L. Warren, J. M. Spurgeon, R. M. Briggs, N. S. Lewis, and H. A. Atwater, "Enhanced absorption and carrier collection in Si wire arrays for photovoltaic applications," *Nature Mater.*, vol. 9, pp. 239–244, 2010.

[5] E. Garnett and P. Yang, "Light trapping in silicon nanowire solar cells," *Nano Lett.*, vol. 10, pp. 1082–1087, 2010.

[6] B. M. Kayes, H. A. Atwater, and N. S. Lewis, "Comparison of the device physics principles of planar and radial p-n junction nanorod solar cells," *J. Appl. Phys.*, vol. 97, pp. 114302–114312, 2005.

[7] J. Zhu and Y. Cui, "Photovoltaics: More solar cells for less," *Nature Mater.*, vol. 9, pp. 183–184, 2010.

[8] W. I. Park, G. Zheng, X. Jiang, B. Tian, and C. M. Lieber, "Controlled synthesis of millimeter-long silicon nanowires with uniform electronic properties," *Nano Lett.*, vol. 8, pp. 3004–3009, 2008.

[9] M. C. Putnam, S. W. Boettcher, M. D. Kelzenberg, D. B. Turner-Evans, J. M. Spurgeon, E. L. Warren, R. M. Briggs, N. S. Lewis, and H. A.

Atwater, "Si microwire-array solar cells," *Energy Environ. Sci.*, vol. 3, pp. 1037–1041, 2010.
[10] O. Gunawan and S. Guha, "Characteristics of vapor-liquid-solid grown silicon nanowire solar cells," *Sol. Energy Mater. Sol. Cells*, vol. 93, pp. 1388–1393, 2009.
[11] X. Li, "Metal assisted chemical etching for high aspect ratio nanostructures: A review of characteristics and applications in photovoltaics," *Current. Opinion Solid State Mater. Sci.*, 2011, DOI: 10.1016/j.cossms.2011.11.002.
[12] X. Li and P. W. Bohn, "Metal-assisted chemical etching in HF/H_2O_2 produces porous silicon," *Appl. Phys. Lett.*, vol. 77, pp. 2572–2574, 2000.
[13] Z. Huang, N. Geyer, P. Werner, J. de Boor, and U. Gösele, "Metal-assisted chemical etching of silicon: A review," *Adv. Mater.*, vol. 23, pp. 285–308, 2011.
[14] W. Chern, K. Hsu, I. S. Chun, B. P. d. Azeredo, N. Ahmed, K.-H. Kim, J.-M. Zuo, N. Fang, P. Ferreira, and X. Li, "Nonlithographic patterning and metal-assisted chemical etching for manufacturing of tunable light-emitting silicon nanowire arrays," *Nano Lett.*, vol. 10, pp. 1582–1588, 2010.
[15] X.-H. Li, R. Song, Y.-K. Ee, P. Kumnorkaew, J. F. Gilchrist, and N. Tansu, "Light extraction efficiency and radiation patterns of III-nitride light-emitting diodes with colloidal microlens arrays with various aspect ratios," *IEEE Photon. J.*, vol. 3, no. 3, pp. 489–499, Jun. 2011.
[16] Y.-K. Ee, P. Kumnorkaew, R. A. Arif, H. Tong, H. Zhao, J. F. Gilchrist, and N. Tansu, "Optimization of light extraction efficiency of III-nitride LEDs with self-assembled colloidal-based microlenses," *IEEE J. Sel. Topics Quantum Electron.*, vol. 15, no. 4, pp. 1218–1225, Jul./Aug. 2009.
[17] M.-A. Tsai, P.-C. Tseng, H.-C. Chen, H.-C. Kuo, and P. Yu, "Enhanced conversion efficiency of a crystalline silicon solar cell with frustum nanorod arrays," *Opt. Exp.*, vol. 19, pp. A28–A34, 2011.
[18] I. S. Chun, E. K. Chow, and X. Li, "Nanoscale three dimensional pattern formation in light emitting porous silicon," *Appl. Phys. Lett.*, vol. 92, pp. 191113–191115, 2008.
[19] J. A. Rogers and R. G. Nuzzo, "Recent progress in soft lithography," *Materials today*, vol. 8, pp. 50–56, 2005.
[20] X. Wang, K. L. Pey, C. H. Yip, E. A. Fitzgerald, and D. A. Antoniadis, "Vertically arrayed Si nanowire/nanorod-based core-shell p-n junction solar cells," *J. Appl. Phys.*, vol. 108, pp. 124303–124307, 2010.
[21] J. Li, H. Yu, S. M. Wong, X. Li, G. Zhang, P. G.-Q. Lo, and D.-L. Kwong, "Design guidelines of periodic Si nanowire arrays for solar cell application," *Appl. Phys. Lett.*, vol. 95, pp. 243113–243115, 2009.
[22] H. Mäckel and R. Lüdemann, "Detailed study of the composition of hydrogenated SiN_x layers for high-quality silicon surface passivation," *J. Appl. Phys.*, vol. 92, pp. 2602–2609, 2002.
[23] T. J. Kempa, B. Tian, D. R. Kim, J. Hu, X. Zheng, and C. M. Lieber, "Single and tandem axial p-i-n nanowire photovoltaic devices," *Nano Lett.*, vol. 8, pp. 3456–3460, 2008.
[24] M. A. Green, "Limits on the open-circuit voltage and efficiency of silicon solar cells imposed by intrinsic Auger processes," *IEEE Trans. Electron Devices*, vol. 31, no. 5, pp. 671–678, May 1984.
[25] M. J. Kerr, A. Cuevas, and P. Campbell, "Limiting efficiency of crystalline silicon solar cells due to Coulomb-enhanced Auger recombination," *Prog. Photovoltaic: Res. Appl.*, vol. 11, pp. 97–104, 2003.
[26] J. del Alamo, S. Swirhun, and R. M. Swanson, "Simultaneous measurement of hole lifetime, hole mobility and bandgap narrowing in heavily doped n-type silicon," in *Proc. Int. Electron Devices Meet.*, 1985, pp. 290–293.
[27] B. Hoex, J. Schmidt, P. Pohl, M. C. M. v. d. Sanden, and W. M. M. Kessels, "Silicon surface passivation by atomic layer deposited Al_2O_3," *J. Appl. Phys.*, vol. 104, pp. 044903–044914, 2008.
[28] I. Martin, M. Vetter, A. Orpella, J. Puigdollers, A. Cuevas, and R. Alcubilla, "Surface passivation of p-type crystalline Si by plasma enhanced chemical vapor deposited amorphous SiC_x:H films," *Appl. Phys. Lett.*, vol. 79, pp. 2199–2201, 2001.
[29] Y. Dan, K. Seo, K. Takei, J. H. Meza, A. Javey, and K. B. Crozier, "Dramatic reduction of surface recombination by in situ surface passivation of silicon nanowires," *Nano Lett.*, vol. 11, pp. 2527–2532, Dec. 2011.

Authors' photographs and biographies not available at the time of publication.